

# RADIATIVE TRANSFER EFFECT ON ULTRAVIOLET PUMPING OF THE 21CM LINE IN THE HIGH REDSHIFT UNIVERSE

LEONID CHUZHUY<sup>1</sup> AND ZHENG ZHENG<sup>2,3</sup>

*Draft version February 5, 2008*

## ABSTRACT

During the epoch of reionization the 21cm signal is sensitive to the scattering rate of the ultraviolet photons, redshifting across the Ly $\alpha$  resonance. Here we calculate the photon scattering rate profile for a single ultraviolet source. After taking into account previously neglected natural broadening of the resonance line, we find that photons approach the resonance frequency and experience most scatterings at a significantly smaller distance from the source than naively expected  $r = (\Delta\nu/\nu_0)(c/H)$ , where  $\Delta\nu = \nu - \nu_0$  is the initial frequency offset, and the discrepancy increases as the initial frequency offset decreases. As a consequence, the scattering rate  $P_\alpha(r)$  drops much faster with increasing distance than the previously assumed  $1/r^2$  profile. Near the source, ( $r \lesssim 1$  comoving Mpc), the scattering rate of photons that redshift into the Ly $\alpha$  resonance converges to  $P_\alpha(r) \propto r^{-7/3}$ . The scattering rate of Ly $\alpha$  photons produced by splitting of photons that redshift into a higher resonance (Ly $\gamma$ , Ly $\delta$ , etc.) is only weakly affected by the radiative transfer, while the sum of scattering rates of Ly $\alpha$  photons produced from all higher resonances also converges to  $P_\alpha(r) \propto r^{-7/3}$  near the source. At  $15 < z < 35$ , on scales of  $\sim 0.01\text{--}20h^{-1}\text{Mpc}$  (comoving), the total scattering rate of Ly $\alpha$  photons from all Lyman resonances is found to be higher by a factor of  $\sim 1 + 0.3[(1+z)/20]^{2/3}$  than obtained without full radiative transfer. Consequently, during the early stage of reionization, the differential brightness of 21cm signal against the cosmic microwave background is also boosted by a similar factor.

*Subject headings:* cosmic microwave background – cosmology: theory – diffuse radiation – intergalactic medium – radio lines: general

## 1. INTRODUCTION

The next generation of radio telescopes (e.g., LOFAR, MWA, SKA, and 21CMA)<sup>4</sup> promises to open a first observational window into the epoch preceding the end of reionization at  $z \gtrsim 6$ . By measuring the redshifted 21cm signal from neutral hydrogen, the new telescopes can provide us with information on the history of reionization, the nature of the first radiation source, the spectrum of the primordial density perturbation field, the cosmological parameters, the physical properties of dark matter particles, etc. (e.g., Madau et al. 1997; Ciardi & Madau 2003; Loeb & Zaldarriaga 2004; Nusser 2005; McQuinn et al. 2006; Barkana & Loeb 2005; Chuzhoy et al. 2006; Shchekinov & Vasiliev 2006).

The 21cm signal can be observed either in absorption or emission against the cosmic microwave background (CMB), when the hydrogen spin temperature,  $T_s$ , is different from the CMB temperature,  $T_{\text{CMB}}$ . The former is defined by the relative populations of the hyperfine states of hydrogen atoms

$$\frac{n_{\text{upper}}}{n_{\text{lower}}} = 3e^{-h\nu_*/kT_s}, \quad (1)$$

where  $\nu_* = 1.4$  GHz is the frequency of hydrogen hyperfine transition. In the high-density gas clouds, which so far have been the only detected sources of the 21cm signal, the decoupling of  $T_s$  from  $T_{\text{CMB}}$  is done by collisions between atoms, which induce direct transitions between the hyperfine states

and couple the spin temperature to the hydrogen kinetic temperature,  $T_k$ . In the intergalactic medium (IGM), on the other hand, after  $z \sim 30$  the density becomes too low for collisional coupling to be effective and the decoupling of  $T_s$  from  $T_{\text{CMB}}$  can be effectively done only by scatterings of Ly $\alpha$  photons, which likewise couple  $T_s$  to  $T_k$  (Wouthuysen 1952). The spin temperature is therefore a weighted function of  $T_{\text{CMB}}$  and  $T_k$  (Field 1958)

$$T_s = \frac{T_{\text{CMB}} + y_\alpha T_k + y_c T_k}{1 + y_\alpha + y_c}, \quad (2)$$

where  $y_c$  is the collisional coupling constant (which we neglect throughout the paper). The radiative coupling constant,  $y_\alpha$ , is

$$y_\alpha = \frac{16\pi^2 T_* e^2 f_{12} J_0}{27 A_{10} T_k m_e c} S_\alpha, \quad (3)$$

where  $f_{12} = 0.4162$  is the oscillator strength of the Ly $\alpha$  transition,  $T_* = h\nu_*/k = 0.068$  K,  $A_{10}$  is the spontaneous emission coefficient of the hyperfine transition and  $J_0$  is the intensity at Ly $\alpha$  resonance, when the backreaction on the incident photons caused by resonant scattering is neglected. For the unperturbed IGM the backreaction correction,  $S_\alpha$ , is (Chuzhoy & Shapiro 2006)

$$S_\alpha = e^{-0.37(1+z)^{1/2} T_k^{-2/3}} \left(1 + \frac{0.4}{T_k}\right)^{-1}. \quad (4)$$

The Ly $\alpha$  photons can be produced in several ways, including recombinations, line cooling, and collisional excitation of atoms by non-thermal electrons produced by X-rays (Chuzhoy et al. 2006; Chen & Miralda-Escudé 2006). However, in case the reionization epoch was dominated by stellar ultraviolet (UV) sources (which at present is the most popular theory) most Ly $\alpha$  photons in the neutral IGM originate as

<sup>1</sup> McDonald Observatory and Department of Astronomy, The University of Texas at Austin, RLM 16.206, Austin, TX 78712, USA; chuzhoy@astro.as.utexas.edu

<sup>2</sup> Institute for Advanced Study, Princeton, NJ, 08540, USA; zhengz@ias.edu

<sup>3</sup> Hubble Fellow

<sup>4</sup> Information on these telescopes can be found at <http://www.lofar.org/>, <http://www.haystack.mit.edu/ast/arrays/mwa/>, <http://www.skatelescope.org/>, and <http://cosmo.bao.ac.cn/project.html/>, respectively.

photons between  $\text{Ly}\alpha$  and Ly-limit frequencies. Due to expansion of the Universe, a fraction of these photons (those emitted between  $\text{Ly}\alpha$  and  $\text{Ly}\beta$ ) would gradually redshift into the  $\text{Ly}\alpha$  resonance. The rest would redshift into one of the higher resonances (generally the one which is just below their initial frequency). The scatterings of high resonance photons produce electron excitations to the  $np$  ( $n > 2$ ) states, which are shortly followed by deexcitations and emission either of the original photon (in case the cascade goes directly to the ground state,  $np \rightarrow 1s$ ) or of several lower energy photons (in case the cascade goes via some intermediate state). Since between  $\sim 12\%$  and  $23\%$  of cascades follow the latter route, after just a few scatterings most of the high resonance photons will be split. Depending on whether the last cascade goes via the  $2p$  or  $2s$  the resulting photons will or will not include a  $\text{Ly}\alpha$  photon.

In this paper, we calculate the  $\text{Ly}\alpha$  scattering rate  $P_\alpha(r)$  as a function of distance  $r$  from the UV radiation source. Contrary to the naive expectation, the scattering rate does not evolve as  $1/r^2$ . While  $P_\alpha(r) \propto 1/r^2$  is a good approximation at low redshifts when hydrogen is mostly ionized, at high redshifts where the Gunn-Peterson optical depth to the  $\text{Ly}\alpha$  photons is extremely large, we find that the scattering rate profile becomes much steeper. Therefore, until the radiation intensity reaches the saturation levels (i.e.,  $y_\alpha \gg T_{\text{CMB}}/T_k$ ), the fluctuations of the 21cm signal would be significantly stronger than previously estimated.

The paper is organized as following. In § 2, we describe our calculation of radiative transfer for “continuum”  $\text{Ly}\alpha$  photons (i.e., photons that gradually redshift into the  $\text{Ly}\alpha$  resonance). In § 3, we describe the radiative transfer of “injected”  $\text{Ly}\alpha$  photons (i.e., photons produced by splitting of high resonance photons). In § 4, we study the total scattering rate from “continuum” and “injected”  $\text{Ly}\alpha$  photons. In § 5, we summarize and discuss our results. Throughout the paper, we adopt a spatially-flat  $\Lambda$ CDM cosmological model with matter density  $\Omega_m = 0.25$  and baryon density  $\Omega_b = 0.044$  in units of the critical density and a Hubble constant  $H_0 \equiv 100h = 72 \text{ km s}^{-1} \text{ Mpc}^{-1}$ , which is consistent with the constraints from the *WMAP* data (Spergel et al. 2007).

## 2. RADIATIVE TRANSFER – “CONTINUUM” PHOTONS

The fate of the UV photon depends on the frequency at which it was emitted. Most photons originally emitted between  $\text{Ly}\alpha$  and  $\text{Ly}\beta$  frequencies will travel a large distance, up to  $(\nu_\beta/\nu_\alpha - 1)c/H(z) \sim 300[(1+z)/26]^{-1/2} \text{ Mpc}$  (comoving), before being scattered by one of the hydrogen atoms. As photon redshifts closer to the  $\text{Ly}\alpha$  resonance its scatterings become more frequent and the mean distance between subsequent scatterings rapidly drops (see Figure 1). Therefore almost all scatterings occur within a very small region<sup>5</sup>. Thus to make an accurate estimate of the scattering rate, it is in practice sufficient to count only scatterings occurring within this region, where photons are very close to the resonance and the number of scatterings is of the order of Gunn-Peterson optical depth. However, to derive the scattering rate profile,  $P_\alpha(r)$ , one also needs to calculate the distance of this region from the radiation source, which by contrast is determined mainly by the first few scatterings before photons redshift into the  $\text{Ly}\alpha$  resonance.

In general, photon scattering cross-section is the function

<sup>5</sup> We find that at  $z \sim 25$  above 99% of the scatterings occur within  $\sim 1.5 \text{ kpc}$  comoving.

of both its frequency and the gas temperature. Neglecting hyperfine splitting, the cross-section without thermal broadening can be written as

$$\sigma(\nu) = \frac{\pi e^2}{m_e c} f \phi(\nu) \quad (5)$$

with the line profile being a Lorentz function

$$\phi(\nu) = \frac{\gamma/4\pi^2}{(\nu - \nu_0)^2 + (\gamma/4\pi)^2}, \quad (6)$$

where  $\nu_0$  is the line-center frequency,  $f$  is the oscillator strength and  $\gamma$  is the spontaneous decay rate ( $\gamma/4\pi \sim 10^{-8}\nu_0$  for  $\text{Ly}\alpha$ ). Thermal broadening introduces a core in the cross-section around the line center with a width of the order of thermal velocity in units of light speed  $c$ , which is about  $10^{-6}$  for the unheated IGM in the redshift range we are interested. In most calculations of the  $\text{Ly}\alpha$  scattering profile around first sources, the line profile  $\phi(\nu)$  is simplified to a Dirac  $\delta_D$  function and scatterings occur as a photon redshifts into line-center frequency. We show in this paper that the frequency dependence of the cross-section affects the scattering rate profile.

Since in the high optical depth regime, the first scatterings happen when photon frequency is still significantly above resonance (i.e., in the Lorentz wing), the distance between the source and the point where photon enters into the resonance is nearly independent of gas temperature. Hence the normalized scattering rate profile is also independent of temperature [though not the total number of scatterings, see eq. (4)]. Since the line frequency offset  $\Delta\nu = \nu - \nu_0$  relevant for our study is much larger than the quantum width and the thermal core width, the cross-section [eq. (5)], being in the wing regime, can be well approximated as

$$\sigma(\nu) = \sigma_c \left( \frac{\Delta\nu}{\nu_0} \right)^{-2}, \quad (7)$$

where  $\sigma_c \propto f\gamma/\nu_0^2$  is formally the scattering cross-section at twice the line-center frequency. We note that in this study, the initial frequency of a photon is blueward of line center, i.e.,  $\Delta\nu > 0$ . This is different from that in Loeb & Rybicki (1999). They investigate the brightness and spectral distributions of escaping  $\text{Ly}\alpha$  radiation around sources before reionization, and in their case photons start at a frequency slightly redward of the resonance, i.e.,  $\Delta\nu < 0$ .

As a photon travels in the neutral medium with Hubble expansion, its frequency redshifts. For a photon with initial frequency offset  $\Delta\nu$ , the scattering optical depth to a distance  $r$  is<sup>6</sup>

$$\tau = \int_0^r n_{\text{HI}} \sigma(\nu - \nu H r/c) dr = \tau_c \beta \left[ \frac{\Delta\nu}{\nu_0} \left( \frac{\Delta\nu}{\nu_0} - \beta \right) \right]^{-1}, \quad (8)$$

where  $n_{\text{HI}}$  and  $H$  are the neutral hydrogen number density and Hubble constant at the redshift in consideration,  $\beta = Hr/c$  and  $\tau_c = n_{\text{HI}} \sigma_c c/H$ . In what follows, we mainly adopt  $\beta$  as the distance variable, which proves to be convenient. At high

<sup>6</sup> We reduce the problem to a calculation for photons traveling in a medium with Hubble expansion velocity field with fixed Hubble constant at a given redshift. Strictly speaking, this approximation is only accurate if the distance traveled is much less than the Hubble radius. Such a condition is slightly broken for the largest scales in the calculation,  $\sim 20\%$  of the Hubble radius (see Fig. 2), which would introduce slight distortions in the scattering rate profiles on these scales. However, for our main purpose, the scales in consideration are generally much smaller and the above approximation is always valid.

redshifts, the conversion from  $\beta$  to comoving distance  $d$  is simply

$$d = 1176\beta \left( \frac{\Omega_m}{0.25} \right)^{-1/2} \left( \frac{1+z}{26} \right)^{-1/2} h^{-1} \text{Mpc}. \quad (9)$$

The parameter  $\tau_c$  can be regarded as a redshift variable for a given cosmology. Formally, it is the optical depth to the Hubble radius seen by a photon with frequency twice the line-center frequency. For Ly $\alpha$  photons, we have

$$\tau_c = 0.0188 \left( \frac{h}{0.72} \right) \left( \frac{\Omega_b}{0.044} \right) \left( \frac{\Omega_m}{0.25} \right)^{-1/2} \left( \frac{1+z}{26} \right)^{3/2}, \quad (10)$$

where the mass fraction of helium is taken to be one quarter.

Equation (8) can be inverted to find the distance traveled by a photon of initial frequency offset  $\Delta\nu/\nu_0$  for a given optical depth  $\tau$ ,

$$\beta = \frac{\Delta\nu}{\nu_0} \left[ 1 - \left( 1 + \frac{\Delta\nu}{\nu_0} \frac{\tau}{\tau_c} \right)^{-1} \right]. \quad (11)$$

For the solution to approach  $\beta = \Delta\nu/\nu_0$ , the one corresponding to a Dirac  $\delta_D$  cross-section, the frequency offset  $\Delta\nu/\nu_0$  needs to be large and/or the parameter  $\tau_c$  needs to be small. In the regime that  $\Delta\nu/\nu_0 \ll \tau_c$ ,  $\beta$  is proportional to  $(\Delta\nu/\nu_0)^2$ , which implies that on sufficiently small scales the distance where most scatterings occur deviates from the expectation with  $\delta_D$  cross-section. The dependence on  $\tau$  in Equation (11) also means that, for a given initial frequency offset, the place where most scatterings occur is no longer at a single distance and instead it has a distribution.

The spherical symmetry and Hubble velocity field allow a simple Monte Carlo calculation of the distribution of Ly $\alpha$  photons from continuum between Ly $\alpha$  and Ly $\beta$  as a function of distance from the central source. The procedure is as follows:

- i. Start a photon from the center ( $\beta_i = 0$ ) with frequency offset  $\Delta\nu/\nu_0$  drawn according to the slope of the UV spectrum of the central source.
- ii. Draw a scattering optical depth  $\tau$  according to the exponential distribution.
- iii. Find the distance  $\beta$  of traveling before scattering according to equation (11).
- iv. Determine the position of scattering,  $\beta_f = \beta_i + \beta$ . That is,  $\beta_f = \sqrt{\beta_i^2 + \beta^2 - 2\beta_i\beta\cos\theta}$ , where  $\cos\theta$  is drawn uniformly between  $-1$  and  $1$ .
- v.  $\Delta\nu/\nu_0 \leftarrow \Delta\nu/\nu_0 - \beta$  (i.e., redshifted) and  $\beta_i \leftarrow \beta_f$ .
- vi. Repeat ii.–v. until  $\Delta\nu/\nu_0$  approaches the width of the thermal core (a few times  $10^{-6}$  for situations here). Then start from i. again until the desired number of photons have been drawn.

The cosmology and redshift are fully encoded in a single parameter  $\tau_c$  [eq. (10)]. In the following discussions, we will assume  $\tau_c = 0.0188$  for Ly $\alpha$  photons, which corresponds to  $z = 25$ . In step iv., we simply assume the direction after scattering is isotropic. We have tested that a more realistic angular distribution, such as a dipole distribution, has little effect on the resultant spatial distribution of Ly $\alpha$  photons.

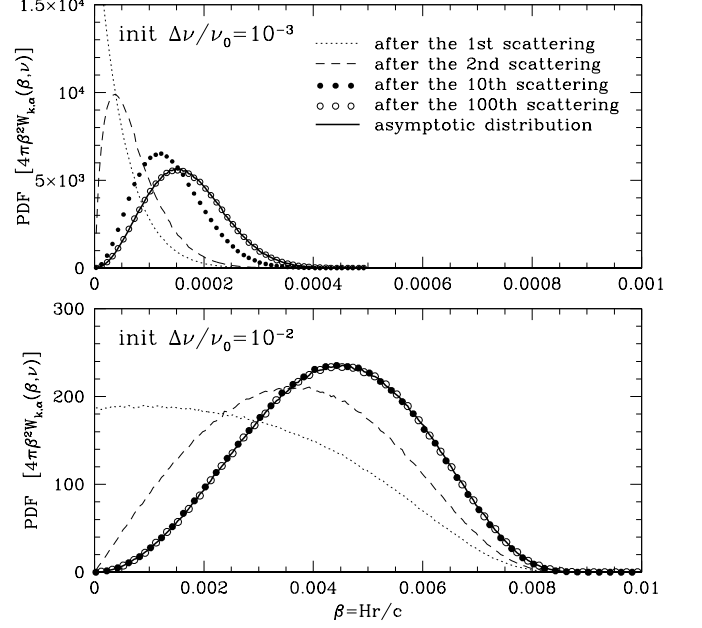


FIG. 1.— Radial probability distribution function (PDF) of “continuum” Ly $\alpha$  photons around a central source at  $z = 25$ , which is proportional to  $r^2$  times the Ly $\alpha$  scattering rate  $P_{\text{cont}}(r)$ . The top and bottom panels are for Ly $\alpha$  photons with initial frequency offset  $\Delta\nu/\nu_0$  of  $10^{-3}$  and  $10^{-2}$ , respectively. The dotted curve, dashed curve, filled circles, and open circles are the distributions after the first, second, 10th and 100th scattering. The solid curve is the asymptotic distribution before core scatterings happen, which is the same profile of the scattering rate for photons with the given initial frequency offset. If a Dirac  $\delta_D$  function is adopted for the scattering cross-section, the distribution would be a spike at the right edge of each panel, with  $Hr/c = \Delta\nu/\nu_0$ .

In Figure 1, we show the spatial distribution of Ly $\alpha$  photons,  $W_{k,\alpha}(r, \nu)$ , after  $k$  scatterings for two initial frequency offsets  $\Delta\nu = \nu - \nu_\alpha$ , based on the above Monte Carlo procedure. The distribution has been normalized so that  $\int 4\pi\beta^2 W_{k,\alpha}(\beta, \nu) d\beta = 1$ . In each panel, the dotted curve, dashed curve, filled circles, and solid circles are the distributions around the central source after the 1st, 2nd, 10th and 100th scattering, respectively. As photons redshift towards the line center, the scatterings become more frequent and the distribution approaches an asymptotic one,  $W_\alpha(r, \nu)$  (thick solid curve). Hence, in practice, to derive the total scattering rate of Ly $\alpha$  photons, it is sufficient to perform the Monte Carlo simulation for the first few scatterings.

If the Ly $\alpha$  scattering is assumed to be a Dirac  $\delta_D$  function, for an initial  $\Delta\nu/\nu_0$  photon, all the scatterings would happen at a distance  $\beta = \Delta\nu/\nu_0$ . However, this is not the case if the frequency dependence of the cross-section is taken into account, as shown in Figure 1 (thick solid curves). The position where most of the scatterings happen is broadly distributed at distances smaller than  $\beta = \Delta\nu/\nu_0$ . Furthermore, the peak of the distribution depends on the initial frequency, the smaller the initial frequency offset  $\Delta\nu/\nu_0$ , the farther away of the peak from the position expected from a  $\delta_D$  function cross-section. For example, as shown in Figure 1, for  $\Delta\nu/\nu_0 = 10^{-2}$ , the peak of the distribution is at a distance  $\sim 45\%$  of that expected from a  $\delta_D$  function cross-section, while for  $\Delta\nu/\nu_0 = 10^{-3}$  it is only  $\sim 15\%$ . As already mentioned, this dependence on initial frequency can be understood by considering the first scattering with equation (11): for a given optical depth  $\tau$ ,  $\beta$  becomes increasingly smaller

than  $\Delta\nu/\nu_0$  as  $\Delta\nu/\nu_0$  becomes smaller. Equation (11) also shows that for smaller  $\tau_c$ , the scattering position would become close to that expected from a  $\delta_D$  function cross-section, which we discuss more about in the next section.

To get the total scattering rate of the “continuum” Ly $\alpha$  photons for a general UV source, one needs to integrate over the frequency range between Ly $\alpha$  and Ly $\beta$

$$P_{\text{cont}}(r) = \tau_{\text{GP}} S_{\alpha} \int_{\nu_{\alpha}}^{\nu_{\beta}} W_{\alpha}(r, \nu) L_{\nu} d\nu, \quad (12)$$

where  $\tau_{\text{GP}}$  is the Gunn-Peterson optical depth to Ly $\alpha$  photons,  $S_{\alpha}$  is the backreaction correction factor [eq. (4)], and  $L_{\nu}$  is the luminosity of the source in terms of number of photons per unit frequency per unit time.

The above dependence of the scattering position on the initial frequency implies that the radial profile of the scattering rate would be steeper than the  $1/r^2$  drop. With the Monte Carlo technique, we calculate the scattering rate profile from “continuum” photons, assuming a flat UV spectrum of the central source (“flat” here means equal number of photons per unit frequency per unit time). In Figure 2, the dashed blue curve is the result from the Monte Carlo simulation, while the dotted blue curve is the corresponding curve of the  $1/r^2$  drop with the same normalization of the UV spectrum of the central source. The true profile is steeper than  $1/r^2$  and the amplitude can be an order of magnitude higher at small distances.

Close to the source the scattering rate scales as  $P_{\text{cont}}(r) \propto r^{-7/3}$ . This behavior can be explained by the following argument. The mean free path  $l$  of the photon emitted with frequency offset  $\Delta\nu$  (i.e., the average distance between subsequent scatterings) scales as  $l \propto (\Delta\nu)^{-2}$  [eq.(11) in the limit of  $\Delta\nu/\nu_0 \ll \tau_c \sim 10^{-2}$ ]. The change of frequency offset between two subsequent scatterings is simply proportional to  $l$ . Therefore the number of scatterings that would occur before the photon frequency moves closer to resonance and its mean free path drops significantly, scales as  $N_{\text{sc}} \propto \Delta\nu/l \propto (\Delta\nu)^{-1}$ . Since the photon direction changes almost at random after each scattering, the total distance it travels until it redshifts into the resonance scales as  $r \propto \sqrt{N_{\text{sc}}} l \propto (\Delta\nu)^{3/2}$ . Conversely, we can say that photons reaching the resonance within distance  $r$  from the source, are emitted with frequency within  $\Delta\nu \propto r^{2/3}$  from Ly $\alpha$  resonance. Since the total number of photons within this frequency range increases in direct proportion with  $\Delta\nu$ , the photon scattering rate, which is proportional to the number of photons reaching the resonance within some region divided by its volume, scales as  $P_{\text{cont}}(r) \propto \Delta\nu/r^3 \propto r^{-7/3}$ .

### 3. RADIATIVE TRANSFER – “INJECTED” PHOTONS

In addition to photons originally emitted between Ly $\alpha$  and Ly $\beta$  frequencies, which redshift into the Ly $\alpha$  resonance, Ly $\alpha$  photons are also produced by splitting of photons originally emitted between Ly $\gamma$  and Lyman-limit frequencies. These photons will be first scattered as they redshift into the closest resonance. In case, following their absorption by a hydrogen atom, the excited electron cascades directly to the ground state, the original photon would be re-emitted. Alternatively, the electron can cascade via some intermediate state, in which case the original photon is split into several photons. Depending on the path of the cascade, the cascade products may include the Ly $\alpha$  photon. The fraction of Ly $\alpha$  photons made up by cascade of high resonances is typically less than  $\sim 15\%$  of the total (Hirata 2006; Pritchard & Furlanetto 2006;

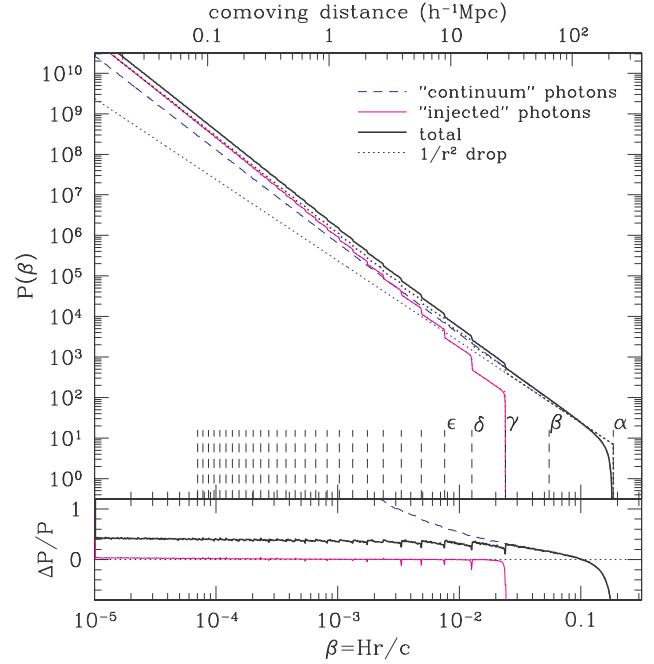


FIG. 2.— The radial profile of Ly $\alpha$  scattering rate around the central source at  $z = 25$  as a sum of contributions from “continuum” and “injected” photons. In the top panel, the blue (dashed), magenta (thin solid), and black (thick solid) curves are those from “continuum” photons and “injected” photons and the total. The corresponding dotted curves are obtained assuming the scattering cross-sections for Lyman lines to be Dirac  $\delta_D$  functions. In the case of the “injected” photons, the dotted curve is almost on top of the magenta (thin solid) curve. Dashed vertical lines mark the maximum distance reached by Lyman series photons with the first five series labeled. In the bottom panel, the fractional differences in the scattering rates with respect to the case of  $\delta_D$  cross-sections are plotted for the “continuum” photons (dashed blue), “injected” photons (thin magenta, near 0), and the sum (thick black), respectively. A flat UV spectrum is assumed (see the text).

Chuzhoy & Shapiro 2007). However, as the distance traveled by photon before it redshifts into the closest  $np$  resonance is of order  $(\nu_{n+1}/\nu_n - 1)c/H \propto n^{-3}$ , the “injected” Ly $\alpha$  photons are produced within much smaller volume and within  $\sim 10$  Mpc (comoving) from the source outnumber the “continuum” Ly $\alpha$  photons (Chuzhoy et al. 2006).

Since the “injected” Ly $\alpha$  photons are injected directly into the resonance (hence their name), to derive their scattering rate profile it is sufficient to follow the path of their high resonance progenitors. The Monte Carlo simulation is similar to what we perform for “continuum” photons, but we need to use cross-sections for higher resonance lines [i.e., different  $\tau_c$  and  $\nu_0$  parameters in eq. (11) for different lines] and record the probability of Ly $\alpha$  production at each scattering. In the calculation, we use the data in Table 1 of Pritchard & Furlanetto (2006) for the probability of decay from the  $np$  state to the ground  $1s$  state and the probability of producing a Ly $\alpha$  photon through cascades from the  $np$  level (also see Hirata 2006). The scattering cross-section for higher resonance Lyman lines are calculated from oscillator strength and Einstein  $A$  coefficient for  $np \rightarrow 1s$  transition listed in Morton (2003) (and extrapolations are used for higher  $n$ ).

The total scattering rate of Ly $\alpha$  photons produced by cascade from  $np$  state with initial frequency  $\nu = \nu_n + \Delta\nu$  is

$$P_{\text{inj},n}(r) = \tau_{\text{GP}} S_{\alpha} \int_{\nu_n}^{\nu_{n+1}} \left[ \sum_{k=1}^{\infty} f_{\alpha,n} f_{\text{des},n} (1 - f_{\text{des},n})^{k-1} W_{k,n}(r, \nu) \right] L_{\nu} d\nu, \quad (13)$$

where  $W_{k,n}(r, \nu)$  is the normalized spatial distribution for Ly $n$

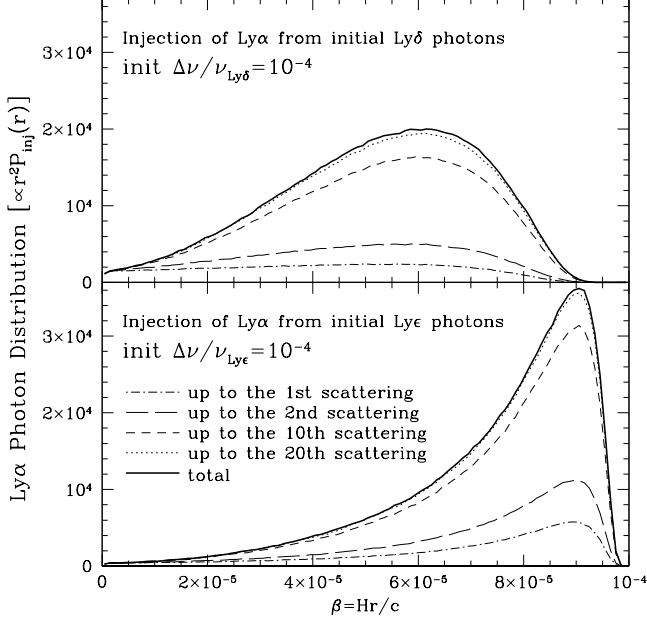


FIG. 3.— Radial distribution of “injected”  $\text{Ly}\alpha$  photons around a central source at  $z = 25$ , which is proportional to  $r^2$  times the  $\text{Ly}\alpha$  scattering rate  $P_{\text{inj}}(r)$ . Shown here are “injected”  $\text{Ly}\alpha$  photons from  $\text{Ly}\delta$  (top panel) and  $\text{Ly}\epsilon$  (bottom panel) resonances with initial frequency offset  $10^{-4}$ . In each panel, the dot-dashed, long dashed, short dashed, and dotted curves are contributions from  $\text{Ly}n$  ( $n = \delta, \epsilon$ ) photons that experience no more than 1, 2, 10, and 20 scatterings before destroyed to produce  $\text{Ly}\alpha$  photons. The thick solid curve is the total contribution from all  $\text{Ly}n$  photons. The distribution from a Dirac  $\delta_D$  cross-section would be a spike at the right edge of each panel, with  $Hr/c = 10^{-4}$ .

photons that experience  $k$  scatterings,  $f_{\text{des},n}$  is the probability that the original  $\text{Ly}n$  photon is destroyed,  $f_{\alpha,n}$  is the chance that the destruction of the  $\text{Ly}n$  photon results in production of the  $\text{Ly}\alpha$  photon (i.e., that the electron cascade goes via  $2p$  rather than  $2s$  state), and other symbols have the same meaning as in equation (12). Since at each scattering there is a significant probability,  $0.12 \lesssim f_{\text{des},n} \lesssim 0.23$ , that the original  $\text{Ly}n$  photon is destroyed, at large values of  $k$ ,  $(1 - f_{\text{des},n})^{k-1}$  approaches zero. That is, the total distribution of “injected”  $\text{Ly}\alpha$  photons can converge by considering those  $np$  photons that experience only a small number of scatterings.

Figure 3 illustrates the evolution of  $\text{Ly}\alpha$  photon distribution for higher resonance photons ( $\text{Ly}\delta$  and  $\text{Ly}\epsilon$ , with initial frequency offset  $10^{-4}$ ) that experience no more than  $k$  scatterings ( $k = 1, 2, 10$ , and  $20$ ) before destroyed. As expected, the distribution approaches quickly to the total distribution (solid curve), similar to the “continuum” case. At the same initial frequency offset, higher resonance photons lead to a peak position closer to that expected from  $\delta_D$  function cross-section. The reason is that a higher resonance line has a smaller cross-section [thus a smaller  $\tau_c$  parameter in eq. (11)].

In contrast to “continuum” photons that typically reach the resonance after multiple scatterings, a photon emitted with frequency blueward of a higher Lyman resonance can produce a resonant  $\text{Ly}\alpha$  photon just after a single scattering. If such a photon has mean free path  $l \propto (\Delta\nu)^2$  as the “continuum” photon case (see § 2), the distance it travels before producing a  $\text{Ly}\alpha$  photon is just  $r \propto l \propto (\Delta\nu)^2$  and one would expect the scattering rate profile  $P_{\text{inj},n}(r) \propto \Delta\nu/r^3 \propto r^{-5/2}$ . However, this can only formally happen extremely close to the central source [ $\Delta\nu/\nu_n \ll \tau_c$ , see eq.(11)] because of the fast drop of

the corresponding  $\tau_c$ , and proximity effect would take over at such scales. Since both the oscillator strength  $f$  and the spontaneous decay rate  $\gamma$  drops as  $n^{-3}$  at large  $n$ , the characteristic scattering optical depth  $\tau_c$  in equation (11) drops as  $n^{-6}$ . Even for  $n = 3$ ,  $\tau_c$  has dropped to a  $10^{-5}$  level. The low value of  $\tau_c$  means that, at a given initial frequency offset, the scattering rate distribution for injected photons is almost the same as that expected from  $\delta_D$  function cross-section with the peak position approaching  $\beta = \Delta\nu/\nu_n$ . For scales of interest (i.e., in the regime of  $\Delta\nu/\nu_n > \tau_c$ ), the mean free path  $l \propto \Delta\nu$  instead of  $(\Delta\nu)^2$  for higher resonance photons, thus each individual  $P_{\text{inj},n}(r)$  follows the  $1/r^2$  profile.

The solid magenta curve in Figure 2 shows the  $\text{Ly}\alpha$  scattering rate profile from injected photons for the same flat UV spectrum of the central source as in the “continuum” case. Each of the steps in the curve reflects the place that a higher resonance line starts to contribute to produce injected  $\text{Ly}\alpha$  photons. At a given initial frequency offset, the scattering rate of injected  $\text{Ly}\alpha$  photons is dominated by those produced by higher level resonance lines. As mentioned above, the location of the injected  $\text{Ly}\alpha$  photons from these resonance lines is close to the expectation of  $\delta_D$ -form cross-section as the corresponding  $\tau_c$  decreases fast. Therefore, the true scattering rate profile is quite close to that from  $\delta_D$ -form cross-section, which is a sum of a series of truncated  $1/r^2$  functions (dotted magenta curve in Figure 2, almost on top of the solid magenta curve). At a distance  $\beta = 10^{-5}$ , the true profile is only higher by  $\sim 4\%$  in this particular case.

Although each individual  $P_{\text{inj},n}(r)$  follows a truncated  $1/r^2$  profile, the overall profile from summing over all “injected” photon contributions no longer follows a  $1/r^2$  profile because the truncation place for the individual component depends on  $n$ . It can be shown that at small scales, the overall profile  $\sum_n P_{\text{inj},n}(r) \propto r^{-7/3}$  (Chuzhoy et al. 2006), interestingly the same dependence as the “continuum” photon case (see § 2). To see this, we note that, with  $r \propto (\nu - \nu_n)/\nu_n$ , the individual component  $P_{\text{inj},n}(r)$  is simply  $\propto L_\nu d\nu/(4\pi r^2 dr) \propto \nu_n/r^2$  for a flat source spectrum  $L_\nu = \text{constant}$  (in photon number per unit frequency per unit time). The slope of the overall profile is then  $-2 + d \ln(\sum_n \nu_n)/d \ln r$ . Since  $\nu_n \propto 1 - 1/n^2$ , we have  $\sum_n \nu_n \propto n$  and  $r \propto 1/n^3$  in the large  $n$  limit. Therefore, the overall profile  $\sum_n P_{\text{inj},n}(r) \propto r^{-7/3}$ , which is what is seen in Figure 2.

#### 4. THE TOTAL SCATTERING RATE

The total scattering rate of  $\text{Ly}\alpha$  photons is obtained after summing over all Lyman series:

$$P_\alpha(r) = P_{\text{cont}}(r) + \sum_{n=3}^{\infty} P_{\text{inj},n}(r). \quad (14)$$

The solid black curve in Figure 2 shows the profile of the total scattering rate. For the case shown here ( $z = 25$ ), “continuum” (“injected”) photons dominate at distances to the center greater (less) than  $\beta \sim 2 \times 10^{-3}$  ( $\sim 3\text{Mpc}$  comoving). At smaller distance, even though the amplitude from “continuum” photons can be an order of magnitude higher than the naive rate given by the  $\delta_D$ -form cross-section, the domination of “injected” photons reduces the difference in the total scattering rate. As for the slope, the overall scattering rate is slightly steeper than the sum of a series of truncated  $1/r^2$  drops (dotted black curve). To the first order, the overall scattering rate is about 40% higher than the naive calculation in a

wide range of distances (see the thick black curve in the lower panel).

The calculation of the scattering rate profile becomes much easier by assuming a  $\delta_D$ -form scattering cross-section. From the above example, we see that to the first order, the exact profile that takes into account the frequency dependence of the cross-section and the radiative transfer effect can be obtained by applying a correction to that from the calculation with  $\delta_D$  cross-section. This correction is almost a constant, increasing the amplitude by a few tens of percent. Apparently, the correction factor depends on redshift, larger at higher redshift because of an increase in the  $\tau_c$  parameter [eq. (11)]. We perform simulations at a series of redshifts and find that the fractional difference  $f_c$  between the exact and the naive calculations of the scattering rate can be approximated as a constant at a given redshift,

$$f_c = 0.381 \left( \frac{1+z}{26} \right)^{0.66}. \quad (15)$$

This approximation underestimates (overestimates) the correction at small (large) scales. For example, at  $z = 25$ ,  $f_c = 44\%$  (32%) at  $\beta = 10^{-5}$  ( $10^{-2}$ ). A more accurate fit that accounts for such a tilt is

$$f_c = 0.364 \left( \frac{1+z}{26} \right)^{0.71} + \left( 0.0115 \frac{z}{25} - 0.0443 \right) \log \frac{\beta}{10^{-3}}, \quad (16)$$

which works almost perfectly for  $15 < z < 35$  and  $10^{-5} < \beta < 10^{-2}$  (roughly corresponding to  $0.01$ – $20 \ h^{-1}\text{Mpc}$  comoving). The first term on the right hand side always dominates and the second term accounts for the slight difference in the slope of the two profiles. With this fitting formula, the profile from the naive calculation can be corrected by multiplying the scattering rate by a factor of  $1 + f_c$ .

All the above examples assume a flat UV spectrum,  $L_\nu \propto \nu^{\alpha_s-1}$  with  $\alpha_s = 1$  between Ly $\alpha$  and Lyman limit, where  $L_\nu$  is the luminosity in terms of number of photons per unit frequency per unit time. The spectrum slope  $\alpha_s$  depends on the nature of the central source. For example, for Population III stars,  $\alpha_s = 1.29$ , while for Population II stars  $\alpha_s = 0.14$  (Barkana & Loeb 2005). Given the narrow frequency range between Ly $\alpha$  and Lyman limit, we do not expect a strong dependence of the scattering rate profile on  $\alpha_s$ . In the case of adopting the  $\delta_D$  cross-section, the scattering rate for an individual component is simply  $\propto L_\nu d\nu / (4\pi\beta^2 d\beta) \propto \nu_0^{\alpha_s} (1 + \beta)^{\alpha_s-1} / \beta^2$ , where the relation  $\beta = (\nu - \nu_0) / \nu_0$  is used. The departure from the  $1/r^2$  drop with respect to the flat spectrum is introduced through  $\nu_0^{\alpha_s}$  and  $(1 + \beta)^{\alpha_s-1}$  and both are small given the narrow frequency range of Lyman series and  $\beta \ll 1$ .

We perform simulations for two cases with quite different spectral slopes,  $\alpha_s = 2$  and  $\alpha_s = 0$ . In Figure 4, we plot ratios of scattering rates for the two cases. The central source luminosity is normalized so that the numbers of photons emitted between Ly $\alpha$  and Lyman limit for the two cases are the same. That's why the  $\alpha_s = 2$  case has a higher rate from “injected” photons (thin solid curve) but lower rate from “continuum” photons (dashed curve). The ratios for the individual components are similar to the  $\delta_D$  cross-section results (dotted curves). However, the steepening of the slope of the scattering rate for the “continuum” photons at small scales, which increases its contribution to the total scattering rate, reduces the difference in the total scattering rates for  $\alpha_s = 2$  and  $\alpha_s = 0$  (thick solid curve). Even with the large difference in the spectral slope, the difference in the overall scattering rates is only

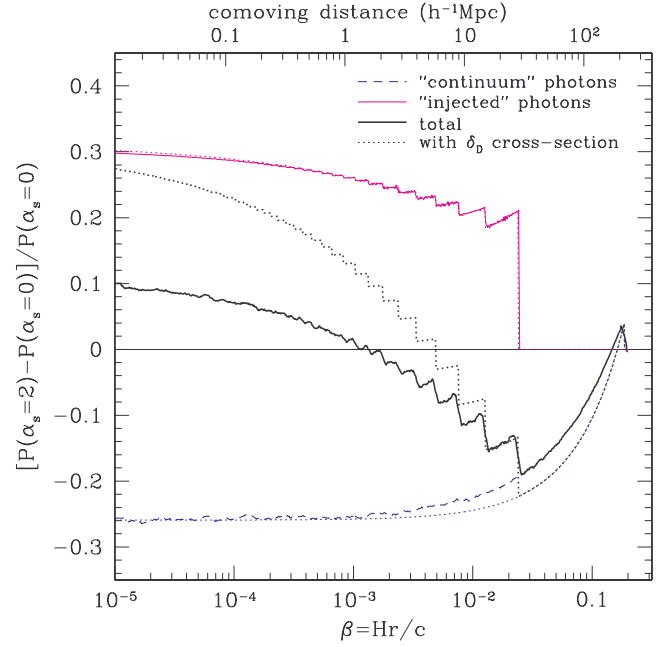


FIG. 4.— Fractional differences in the scattering rate profiles for different slopes of central source spectra at  $z = 25$ . The luminosity of the central source (number of photons per unit frequency per unit time) between Ly $\alpha$  and Lyman limit is assumed to follow  $L_\nu \propto \nu^{\alpha_s-1}$  with  $\alpha_s = 2$  and  $0$ , respectively. The spectra are normalized to have the same number of photons between Ly $\alpha$  and Lyman limit. The dashed and thin solid curves are for rates from “continuum” and “injected” photons, respectively, and the thick solid curves is for the total rate. Dotted curves are for the corresponding cases with Dirac  $\delta_D$  cross-sections.

at a level less than 10% for  $\beta < 10^{-2}$ . A comparison between cases using spectral slopes of Population II ( $\alpha_s = 0.14$ ) and Population III ( $\alpha_s = 1.29$ ) stars shows a pattern similar to what is seen in Figure 4 with the difference in the overall scattering rates being at a level of 5%.

## 5. SUMMARY AND DISCUSSION

We investigate the effects of frequency dependence of scattering cross-section and radiative transfer on the scattering rate profile of Ly $\alpha$  photons around a central UV source, which is relevant for the pumping of the 21cm line in the high redshift universe.

Because of the frequency dependence of the scattering cross-section, a photon between Ly $\alpha$  and Ly $\beta$  frequency (“continuum” Ly $\alpha$  photon) experiences a small number of wing scatterings before it redshifts to the core frequency and starts core scattering. Core scatterings, which determine the scattering rate, happen at distances much less than that expected from a  $\delta_D$  scattering cross-section. For scatterings of higher resonance photons that produce “injected” Ly $\alpha$  photons, the effect is weak owing to the fast drop in the cross-section. We have shown that for a single UV source the scattering rate profile of “continuum” Ly $\alpha$  photons is significantly steeper than  $1/r^2$  (previously expected from  $\delta_D$  scattering cross-section), approaching  $r^{-7/3}$  near the source. The scattering rate profile of “injected” Ly $\alpha$  photons from an individual high Lyman resonance closely follows a truncated  $1/r^2$  profile, while the overall profile from all higher Lyman resonances coincidentally also approaches  $r^{-7/3}$  near the source. At  $15 < z < 35$ , the total scattering rate from “continuum” and “injected” photons is 30–50% higher than the naive calculation that adopts  $\delta_D$  cross-sections, on scales of  $\sim 0.01$ –



$20h^{-1}\text{Mpc}$  (comoving). We also find that, when radiative transfer effects are properly accounted for, the slope of the scattering rate profile does not have a strong dependence on the spectral slope of the central source.

In our calculations we have assumed that during the early stages of reionization the gas temperature changes adiabatically. If instead, the gas was significantly heated, the Doppler core for  $\text{Ly}\alpha$  photons would be increased and their scattering rate profile would be even steeper. However, since the temperature of neutral hydrogen does not exceed  $\sim 10^4$  K, the scales above  $\sim 100$  kpc (comoving) would be virtually unaffected.

As a consequence of the higher scattering rate with respect to the naive calculation, the spatial fluctuations in the pumping radiation field produced by multiple UV sources would be significantly higher as well. During the early stages of reionization, when the UV intensity is relatively low, the differential brightness of the 21cm signal scales almost linearly with the scattering rate of the  $\text{Ly}\alpha$  photons and the corrections to the scattering rate translate into similar corrections to the 21cm brightness. Such a correction would increase the size of the expected  $\text{Ly}\alpha$  spheres around first sources (e.g., Cen

2006; Chen & Miralda-Escudé 2006). Moreover, if the radiative transfer effect is overlooked, the fluctuation power spectrum estimated from 21cm observations would be skewed on scales up to a few tens of Mpc, which would lead to inaccurate inference of the matter fluctuation power spectrum (such as the amplitude and the running of the spectral index). Therefore, until the epoch when the intensity of pumping radiation reaches a saturation level (if such epoch in fact exists), the correct interpretation of the 21cm signal requires taking into account radiative transfer (mainly for “continuum”  $\text{Ly}\alpha$  photons), as described in this paper.

We thank Chris Hirata and Jordi Miralda-Escudé for useful discussions. L.C. thanks the McDonald Observatory for the W.J. McDonald Fellowship. Z.Z. acknowledges the support of NASA through Hubble Fellowship grant HF-01181.01-A awarded by the Space Telescope Science Institute, which is operated by the Association of Universities for Research in Astronomy, Inc., for NASA, under contract NAS 5-26555.

#### REFERENCES

- Barkana, R., & Loeb, A. 2005, 626, 1  
 Cen, R. 2006, ApJ, 648, 47  
 Chen, X., & Miralda-Escudé, J. 2006, ArXiv Astrophysics e-prints, arXiv:astro-ph/0605439  
 Chuzhoy, L., Alvarez, M., & Shapiro, P. R. 2006, ApJ, 648, L1  
 Chuzhoy, L. & Shapiro, P. R. 2006, ApJ, 651, 1  
 Chuzhoy, L. & Shapiro, P. R. 2007, ApJ, 655, 843  
 Ciardi, B., & Madau, P., 2003, ApJ, 596, 1  
 Field, G. B. 1958, Proc. IRE, 46, 240  
 Hirata, C.M. 2006, MNRAS, 367, 259  
 Loeb, A., & Rybicki, G. B. 1999, ApJ, 524, 527  
 Loeb, A., & Zaldarriaga, M. 2004, Phys. Rev. Lett., 92, 211301  
 Madau, P., Meiksin, A., & Rees, M. J. 1997, ApJ, 475, 429  
 McQuinn, M., Zahn, O., Zaldarriaga, M., Hernquist, L., & Furlanetto, S. R. 2006, ApJ, 653, 815  
 Morton, D. C. 2003, ApJS, 149, 205  
 Nusser, A. 2005, MNRAS, 364, 743  
 Pritchard, J. R., & Furlanetto, S. R. 2006, MNRAS, 367, 1057  
 Shchekinov, Yu. A., & Vasiliev, E. O. 2006, astro-ph/0604231  
 Spergel, D. N., et al. 2007, ApJS, 170, 377  
 Wouthuysen, S. A. 1952, AJ, 57, 31